Nanoscale

PAPER

View Article Online
View Journal | View Issue

Check for updates

Cite this: *Nanoscale*, 2023, **15**, 3351

Towards site-specific emission enhancement of gold nanoclusters using plasmonic systems: advantages and limitations†

Ondrej Pavelka, [a] Sergey Dyakov,[b] Klaudia Kvakova,[c,d] Jozef Vesely,[e] Petr Cigler[c] and Jan Valenta *[a]

Photoluminescent gold nanoclusters are widely seen as a promising candidate for applications in biosensing and bioimaging. Although they have many of the required properties, such as biocompatibility and photostability, the luminescence of near infrared emitting gold nanoclusters is still relatively weak compared to the best available fluorophores. This study contributes to the ongoing debate on the possibilities and limitations of improving the performance of gold nanoclusters by combining them with plasmonic nanostructures. We focus on a detailed description of the emission enhancement and compare it with the excitation enhancement obtained in recent works. We prepared a well-defined series of gold nanoclusters attached to gold nanorods whose plasmonic band is tuned to the emission band of gold nanoclusters. In the resultant single-element hybrid nanostructure, the gold nanorods control the luminescence of gold nanoclusters in terms of its spectral position, polarization and lifetime. We identified a range of parameters which determine the mutual interaction of both particles including the inter-particle distance, plasmon–emission spectral overlap, dimension of gold nanorods and even the specific position of gold nanoclusters attached on their surface. We critically assess the practical and theoretical photoluminescence enhancements achievable using the above strategy. Although the emission enhancement was generally low, the observations and methodology presented in this study can provide a valuable insight into the plasmonic enhancement in general and into the photophysics of gold nanoclusters. We believe that our approach can be largely generalized for other relevant studies on plasmon enhanced luminescence.

Received 29th November 2022,
Accepted 9th January 2023

DOI: 10.1039/d2nr06680g

rsc.li/nanoscale

Open Access Article. Published on 09 January 2023. Downloaded on 5/9/2026 9:48:21 AM.
This article is licensed under a Creative Commons Attribution-NonCommercial 3.0 Unported Licence.

Introduction

Ultra-small photoluminescent gold nanoclusters (AuNCs) are a group of red to near-infrared emitters[1–5] with a rapidly broadening field of applications.[6,7] Due to their strong quantum confinement effects (the diameter of the Au core is typically <2 nm) and various possibilities of atomic arrangements of their cores, AuNCs show characteristic, molecule-like optical, magnetic, and electronic properties such as optical chirality,[8,9] ferromagnetism,[10,11] and size dependent photoluminescence (PL).[6,12,13] Furthermore, the AuNC PL can be tuned by the ligands used for AuNC surface capping.[14–17] In combination with good biocompatibility[18] and reasonable photostability,[19] AuNCs are a promising candidate for use in sensing[20–22] and biotechnology.[23–25] The limiting factor for the potential applicability of AuNCs is their modest quantum yield (QY) which is usually below 10%[26,27] and can be improved by appropriate ligand design.[1] Nevertheless, compared to the currently available most efficient NIR-emitting quantum dots (QY up to 80%),[28–31] the brightness of AuNCs leaves plenty of room for improvement.

One of the widely explored techniques for improving the performance of photoluminescent agents is their combination with plasmonic nanostructures.[32–34] The so-called plasmon enhanced PL can in principle originate from two different processes. Localized surface plasmon resonance (LSPR) can either increase the effective absorption cross section of fluorophores (referred to as excitation enhancement) or accelerate their radiative recombination rate by increasing the local density of states (referred to as emission enhancement). Both types of

[a]*Department of Chemical Physics and Optics, Faculty of Mathematics and Physics, Charles University, Ke Karlovu 3, 121 16 Prague, Czechia. E-mail: jan.valenta@mff.cuni.cz*
[b]*Photonics & Quantum Materials Center, Skolkovo Institute of Science and Technology, Nobel Street 3, Moscow 143025, Russia*
[c]*Institute of Organic Chemistry and Biochemistry of the Czech Academy of Sciences, Flemingovo nam. 2, 166 10 Prague, Czechia*
[d]*Institute of Medical Biochemistry and Laboratory Diagnostics, First Faculty of Medicine, Charles University, Katerinska 1660/32, Prague 121 08, Czechia*
[e]*Department of Physics of Materials, Faculty of Mathematics and Physics, Charles University, Ke Karlovu 3, 121 16 Prague, Czechia*

† Electronic supplementary information (ESI) available. See DOI: https://doi.org/10.1039/d2nr06680g

Open Access Article. Published on 09 January 2023. Downloaded on 5/9/2026 9:48:21 AM.
This article is licensed under a Creative Commons Attribution-NonCommercial 3.0 Unported Licence.

enhancements have been previously explored for various combinations of noble metal nanoclusters and plasmonic nanoparticles.[35–44] However, there is no clear consensus on what effect the introduction of plasmonic particles has as both PL enhancement[35–39] and quenching have been reported.[40–44]

In our recent work,[45] we contributed to this discussion by studying the excitation enhancement in AuNCs attached to silica (SiO_2) coated gold nanorods (AuNRs). By carefully evaluating the stoichiometry of the resultant core@shell nanoparticles (AuNRs@AuNCs) we were able to come up with a calibrated PL enhancement measurement which yielded enhancement factors up to 4.4×. In this study we use the same combination of nanoparticles to investigate the emission enhancement in AuNCs. This is enabled by a wide tunability of the stronger, longitudinal plasmonic band of AuNRs (LSPR), which can be shifted from the region of AuNC absorption (as used for excitation enhancement) to the region of AuNC emission. Such a setting leads to an increased radiative recombination rate in AuNCs placed in the vicinity of AuNRs, traditionally known as the Purcell effect and described by the (total) Purcell factor (f_{tot}). However, due to losses caused by energy transfer and absorption in the plasmonic particles, only part of the accelerated radiation is outcoupled to the far field (described by the external Purcell factor f_{ext}). In the end, it is the interplay between the gains and losses caused by the plasmonic particles that decides the resultant PL enhancement or quenching.

Although the modified QY of AuNCs attached to AuNRs can be theoretically calculated for a known combination of f_{tot} and f_{ext} (see eqn (14), the model presented in the ESI†), finding it experimentally is extremely challenging.[46] As an alternative, the effect of AuNRs can be assessed by comparing the PL intensity from samples with calibrated amounts of bare and modified AuNCs. Still, as we show in this study, such evaluation must be performed with care and all contributing factors have to be considered. Thus, apart from standard parameters such as the AuNC–AuNR distance, we discuss the influence of the used spacer, PL–LSPR overlap, AuNR volume and even a specific position of AuNCs on the surface of AuNRs.

An overview of the experimental situation discussed in this work is shown in Fig. 1. The tunable longitudinal LSPR band of AuNRs overlaps with the emission band of AuNCs, while the excitation wavelength is chosen not to match either of the plasmonic resonances of AuNRs (see Fig. 1a). Therefore, no significant excitation enhancement of PL is expected. Due to the shape anisotropy of AuNRs, the spatial profile of the local density of states associated with their longitudinal LSPR band is inhomogeneous, with the density being higher near the AuNR tips. The same spatial inhomogeneity is then translated into the Purcell factor and the resulting PL emission enhancement. This is qualitatively shown in Fig. 1b, which displays a map of the external Purcell factor at variable distances and positions around AuNRs. Assuming that AuNCs distributed homogeneously on the whole surface of the AuNRs (schematically illustrated in Fig. 1c; experimental result in Fig. 1e), higher PL enhancement is expected for AuNCs near the AuNR tips (Fig. 1d). As a result, the position of AuNCs on the surface of AuNRs represents an additional parameter in the PL enhancement studies.

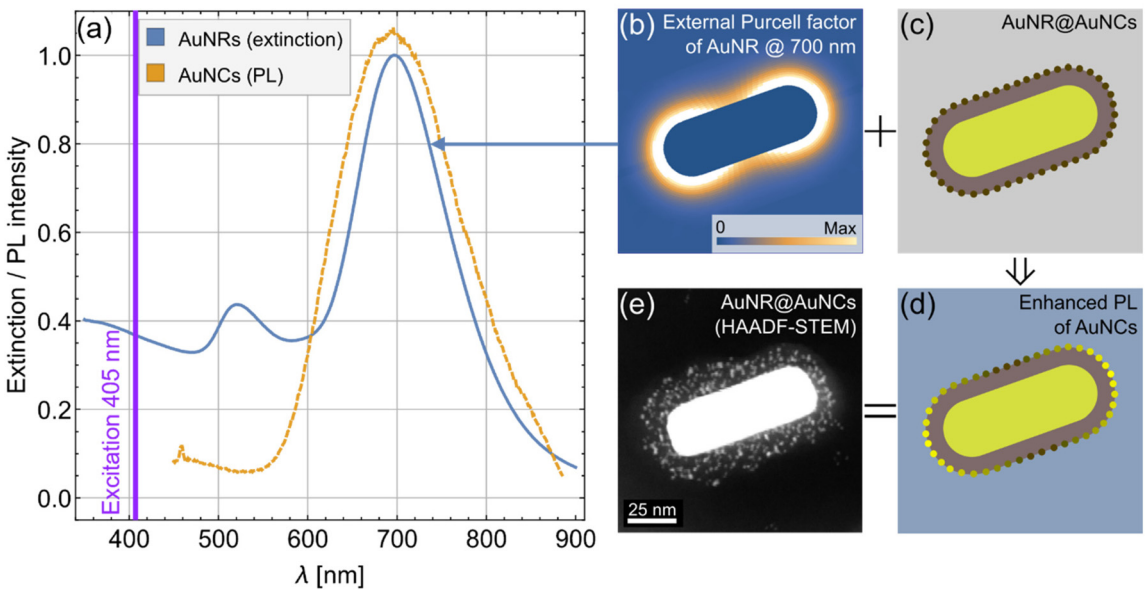

Fig. 1 An overview of the plasmonic emission enhancement in AuNCs by AuNRs. (a) The longitudinal LSPR band of AuNRs and the PL band of AuNCs overlap at 700 nm. The excitation wavelength (405 nm) does not match either of the LSPR bands of AuNRs. (b) Map of the external Purcell factor around a single AuNR (see the ESI† for details of the calculation). (c) A homogeneous coverage of an Au@SiO_2 NR by AuNCs can be assumed as confirmed by (e) HAADF-STEM imaging. Note that a 2D projection of a 3D object is shown in (e), causing AuNCs seemingly appear at variable distances from the AuNR. (d) Based on the findings shown in (b) + (c), a site-specific interaction between AuNR and AuNCs is expected with a higher PL enhancement near the tips of the AuNR.

This journal is © The Royal Society of Chemistry 2023

Open Access Article. Published on 09 January 2023. Downloaded on 5/9/2026 9:48:21 AM.
This article is licensed under a Creative Commons Attribution-NonCommercial 3.0 Unported Licence.

Experimental

Synthesis of nanoparticles

Functionalized AuNCs were prepared according to a previously published procedure.[47] Briefly, the AuNCs were capped with a combination of thioctic acid and thiolated poly(ethylene glycol). The AuNCs were then further modified with the 3-(aminopropyl)triphenylphosphonium cation, which is responsible for the positive surface charge of functionalized AuNCs. High resolution TEM (HRTEM) and additional characterization of the particles can be found in a previous report.[1] The concentration of AuNCs was determined from the total concentration of Au in the solution (as determined by ICP OES) and the average diameter of AuNCs (≈1.2 ± 0.2 nm) obtained from HRTEM.

The synthesis of AuNRs was based on the well-established seeded growth method,[48] which uses cetyltrimethylammonium bromide (CTAB) as a capping agent. The aspect ratio of the AuNRs was controlled by the concentration of silver nitrate and by slow addition of the gold salt into the growth solution as described in our previous report.[49] The dimensions of the AuNRs were measured from SEM images by analyzing more than 200 particles. The concentrations of AuNRs in the solution were estimated from extinction measurements using an empirical formula published by Edgar *et al.*[50] and by assuming the AuNR shape to be cylindrical with hemispherical caps. As noted in our previous work,[49] such calculation agrees very well with results of the more accurate ICP OES and can therefore be used instead. For coating the AuNRs with silica (SiO_2), the previously published protocol was used,[49] yielding homogeneous shells even at a low thicknesses of several nanometers. Two set (8 + 7) samples of silica-coated AuNRs (Au@SiO_2 NRs) were prepared with the silica shell thicknesses ranging from 5 to 23 nm for PL lifetime measurements, and 4 to 13.5 nm for PL enhancement measurements, respectively. All samples were characterized using SEM and/or transmission electron microscopy (TEM) analogously to our previous report[49] and some of the samples were also characterized by ζ-potential measurement in a 2 pM aqueous solution of the particles at 25 °C in a dip cell (Zetasizer Nano ZS, Malvern Instruments).

The as prepared Au@SiO_2 NRs were stabilized by CTAB and have positive ζ-potential (≈50 mV).[51] Mixing them with the positively charged AuNCs therefore yields no permanent connection between the two types of particles. Such CTAB-stabilized particles were used for preparation of a control sample (denoted as AuNRs + AuNCs) where AuNCs are not attached to the AuNRs.[49] However, silica coating enables the transfer of Au@SiO_2 NRs into ethanol, where their ζ-potential turns to negative (≈−25 mV)[49] and thus allows the electrostatic binding of AuNCs. This approach was used for the preparation of a serious of AuNRs@AuNCs.

For reference experiments, spherical SiO_2 nanoparticles (SiO_2NPs) attached with AuNCs (SiO_2NPs@AuNCs), and SiO_2-coated spherical Au nanoparticles (AuNPs) attached with AuNCs (AuNPs@AuNCs) were also prepared. Monodisperse spherical SiO_2NPs were prepared using the Stöber procedure[52] (see Fig. S10† for TEM). The particles showed a ζ-potential of −48 ± 1 mV in aqueous solution. The electrostatic adsorption of AuNCs on the SiO_2NPs led to a strong charge compensation, resulting in a ζ-potential of 0.09 ± 0.08 mV of the SiO_2NPs@AuNCs.

AuNPs were prepared in accordance with the protocol introduced by Turkevich *et al.*[53] This procedure yields AuNPs stabilized by sodium citrate, which in our case had a mean diameter of 30 nm. AuNPs were transferred to 1 mM CTAB solution through one round of centrifugation (8000*g*, 20 min, 27 °C) upon which the same protocol for silica coating was applied as for AuNRs. The electrostatic adsorption of AuNCs on the silicated surface provided AuNPs@AuNCs and showed a similar charge compensation as observed for SiO_2NPs@AuNCs.

Electron microscopy

Images of AuNRs for measuring dimensions were obtained using an Auriga Compact SEM (Zeiss) microscope operated at 7–15 kV. The images of Au@SiO_2 NRs and AuNRs@AuNCs were recorded on a JEOL JEM-2200FS microscope operated at 200 kV. HAADF-STEM mode was used to enhance the contrast between AuNCs and SiO_2 shells in most of the characterization studies. Solutions with particles were drop-casted on a silicon wafer or lacey carbon coated copper grids (SPI) for SEM and TEM analysis, respectively.

Optical spectroscopy

Extinction spectra of the solutions were recorded with a Specord 250 spectrophotometer (Analytik Jena). PL and dark field (DF) spectra were recorded using a custom-built microspectroscopy setup based on an inverted optical microscope with a spectrometer and a liquid-nitrogen-cooled CCD camera.[54] CW 405 nm and 510 nm lasers were used for PL excitation and a halogen lamp was used for DF excitation, respectively. For measurements at a single particle level a dilute solution of AuNRs@AuNCs in ethanol was drop-casted on a glass slide. Fast evaporation of ethanol yielded regions with well separated particles.

Calibrated PL intensity enhancement measurements were performed with solutions of AuNRs@AuNCs. In a typical experiment, the PL spectra were collected from a ≈300 µl volume of AuNRs@AuNCs placed in a quartz cuvette (optical path length of 1 mm). The excitation intensity was limited to ensure that absorption saturation in AuNCs was avoided. Cuvettes were cleaned with aqua regia between individual measurements to remove all AuNCs that could potentially remain attached at the walls of the cuvettes.

PL quantum yield determination

The PL QY of the initial AuNC solution was measured using an integrating sphere (IS) (d = 10 cm, Sphere Optics) with tunable excitation by a laser-driven light source (EQ-99X-S, Energetiq) connected to a 15 cm monochromator (SP-2150i, Acton). Both excitation and emission light was guided to IS and out from IS using silica fiber bundles. The output fiber was coupled to the

Open Access Article. Published on 09 January 2023. Downloaded on 5/9/2026 9:48:21 AM.
This article is licensed under a Creative Commons Attribution-NonCommercial 3.0 Unported Licence.

detection system of the above described micro-spectroscopy setup. The whole system was calibrated using the standard of spectral irradiance (Oriel 63360).[49]

PL lifetime measurements

PL lifetime measurements were performed *via* time-gated imaging.[55] 10 μs pulses of a 405 nm laser were used for excitation and an ICCD camera was used for imaging. The time gate width was usually set to 50 ns and 65 000 frames were accumulated for each delay. At least 8 different spots on the substrate were studied for each sample with 20–100 emission sources on each spot. A summed signal from all the single sources was used for average lifetime fitting and calculations. More details on the method of PL lifetime calculations can be found in our previous study.[49]

Numerical simulations

For numerical simulations, PL was approximated by the radiation of oscillating electric dipoles that are placed near AuNRs. The Purcell factor and excitation efficiency of dipoles in the vicinity of AuNRs were calculated with the boundary element method (BEM)[56] using the MNPBEM toolbox.[57,58] More details about the simulations and theoretical model for the calculations can be found in the ESI.†

Results and discussion

Preparation and basic characterization of AuNRs@AuNC ensembles

Two types of AuNRs, which differ in the spectral position of their longitudinal LSPR bands, were used in our experiments. The first type of AuNRs, denoted as AuNRs 1, exhibits a longitudinal LSPR band that nearly perfectly matches the emission band of AuNCs at ≈700 nm. This represents the optimal situation shown in Fig. 1a. The other type of nanorods, denoted as AuNRs 2, exhibits a longitudinal LSPR band that is redshifted from the center of the PL of AuNCs but still partially overlaps with it at ≈750 nm. The full characterization of AuNRs 1 and 2 is in shown Fig. S1a (in the ESI†), which shows their extinction spectra and size distributions. Using these data, the different positions of the longitudinal LSPR peaks are explained by the different aspect ratios of the two types of AuNRs, which yield 2.7 for AuNRs 1 and 3.2 for AuNRs 2. Although AuNRs 1 are clearly more suitable for achieving the maximum PL emission enhancement in AuNCs, we show in the following that the spectral offset created for AuNRs 2 opens a path towards a deeper understanding of the site specificity of the enhancement discussed in the Introduction section of this study.

The synthesis of AuNRs@AuNCs in this study is based on the results of our recent work, where we studied plasmonic excitation enhancement on the same type of hybrid particles.[45] First, silica shells were grown on AuNRs, forming a transparent tunable spacer between AuNRs and AuNCs. To monitor the influence of the AuNR–AuNC distance on the PL enhancement, a wide range (5–28 nm) of SiO_2 shell thicknesses was prepared. Representative SEM images of all SiO_2 coated AuNRs (Au@SiO_2 NRs) prepared from AuNRs 2 are shown in Fig. S2 (in the ESI†), proving a good uniformity of the SiO_2 shells at all thicknesses. As a second step, AuNCs were attached to Au@SiO_2 NRs by mixing the two respective solutions together and using the opposite surface charge of the two types of particles. Previously, a thorough characterization using a combination of complementary techniques (such as TEM imaging, PL measurements, and neutron activation radiolabeling) enabled us to draw several important conclusions about the AuNRs@AuNCs prepared in this way:

(1) the electrostatic attraction between the positively charged AuNCs and the negatively charged silica surface of AuNRs is sufficiently strong for the permanent attachment of AuNCs to Au@SiO_2 NRs.

(2) Unbound AuNCs can be efficiently removed from the solution of AuNRs@AuNCs by centrifugation without affecting the AuNCs that were already attached.

(3) There is an upper limit for the number of AuNCs that can be attached to a unit surface of Au@SiO_2 NRs, yielding approximately 20% surface coverage of Au@SiO_2 NRs by AuNCs. With AuNR dimensions used in our work, this corresponds to $\approx 10^3$ of AuNCs per single AuNR. Importantly, AuNCs remain exclusively on the surface of the SiO_2 shells and do not penetrate into their volume. This ensures a good control of the distance between AuNCs and AuNRs.

(4) Particles with partial AuNC loading can be prepared when a sublimit amount of AuNCs is mixed with Au@SiO_2 NRs. Conveniently, the capture of the AuNCs by the SiO_2 surface is quantitative, so the number of non-attached AuNCs is negligible. In this situation, no centrifugation of the solution is thus required.

All these findings serve as an important precondition for the validity of the results of the optical experiments presented in this study. Given that the only difference between AuNRs@AuNCs used here and in our previous report is the aspect ratio of AuNRs, we assume the validity of the claims in (1)–(4) with no further evidence. The achieved quality of the prepared AuNRs@AuNCs is evidenced by the HAADF-STEM images in Fig. S3 (in the ESI†), where rich and homogeneous AuNC loading is shown for three SiO_2 shell thicknesses (6.5, 11, and 17 nm). Importantly, these images also demonstrate that regardless of the thickness, the uniformity of the shells is sustained even after AuNC attachment.

The main objective of this work is to study the PL emission enhancement of AuNCs by AuNRs. This type of enhancement is caused by the Purcell effect, where the radiative recombination rate in AuNCs is accelerated by the plasmonic modes of AuNRs. Consequently, the PL emission is coupled to the LSPR of AuNRs and the optical response of AuNRs then determines the optical response of the whole AuNC–AuNR hybrid system. In practice, this is often demonstrated by a spectral shift of the PL towards the plasmonic resonance (in the cases where some offset between the PL and LSPR bands is present) and by the alignment of PL and LSPR polarizations.[59]

 This journal is © The Royal Society of Chemistry 2023

Open Access Article. Published on 09 January 2023. Downloaded on 5/9/2026 9:48:21 AM.
This article is licensed under a Creative Commons Attribution-NonCommercial 3.0 Unported Licence.

Single particle scattering and photoluminescence

Following this theory, the coupling between the PL of AuNCs and LSPR of AuNRs was first examined to make sure that our design of AuNRs@AuNCs meets the conditions for emission enhancement. In this experiment, a solution of AuNRs@AuNCs with a low particle concentration was drop-casted on a glass slide to create spots enabling investigation at a single particle level. Dark field (DF) scattering spectra and PL spectra were collected from the same spot and their polarization dependence was monitored (see the Experimental section for the details of the experimental setting). A representative result is shown in Fig. 2, which shows an example of the spectra measured for a sample of AuNRs@AuNCs prepared from AuNRs 2 with a 11 nm SiO_2 shell. The DF scattering spectra (Fig. 2a) have two major peaks at ≈705 and ≈770 nm, indicating that the signal was collected from at least two different particles (or two small groups of particles). Taking the maximum intensities of these two peaks at varying polarization angles, ϕ generates datapoints as shown in Fig. 2b. Both of these sets of datapoints are well reproduced by a $\sim\cos^2(\phi)$ function (solid lines in Fig. 2b), which, as expected, demonstrates that the scattering associated with the longitudinal LSPR of AuNRs is linearly polarized. Note that the polarization dependencies are offset from each other by ≈π/2. Considering that the polarization of the longitudinal LSPR mode is along the longer axis of AuNRs, this can be explained as the observation of two perpendicularly oriented AuNRs (or groups of AuNRs with perpendicular dominant orientations). Importantly, the same features are recognized also in the corresponding PL spectra in Fig. 2c and d. The two major PL peaks at ≈710 and 770 nm match the spectral positions of DF scattering peaks nearly perfectly and also their polarization dependence shows the same pattern. The only difference is a gradual attenuation of the PL signal (see the decreased PL intensity at $\phi = \pi$ compared to the intensity at $\phi = 0$) caused by long exposure times during the measurement. The datapoints in Fig. 2d were therefore fitted with a modified function which accounts for the attenuation but keeps the same periodicity. This is explained in more detail in the ESI,† where another example of a spectral and polarization match between the PL and DF scattering of AuNRs@AuNCs is also shown (Fig. S4†).

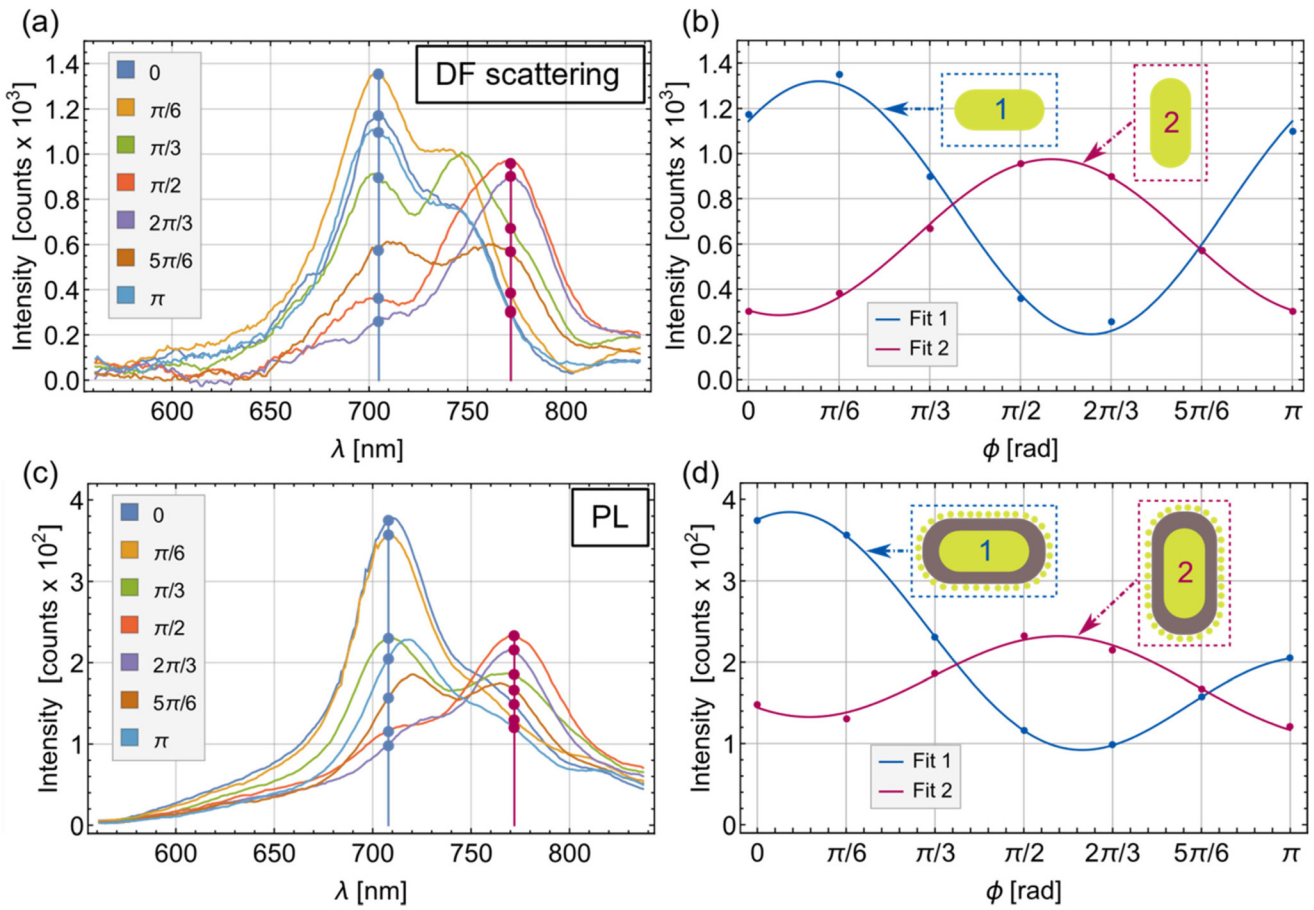

Fig. 2 Single particle measurement of (a and b) DF scattering and (c and d) PL spectra of AuNRs@AuNCs for different polarizations. AuNRs 2 with a 11 nm silica shell was used. Peak values from (a) and (c) are plotted as a function of polarization in (b) and (d), respectively, to visualize the same polarization dependency of PL and DF scatterings for either of the observed peaks at 700 and 770 nm.

Open Access Article. Published on 09 January 2023. Downloaded on 5/9/2026 9:48:21 AM.
This article is licensed under a Creative Commons Attribution-NonCommercial 3.0 Unported Licence.

The results presented in Fig. 2 and S4† suggest a successful establishment of coupling between the PL of AuNCs and the LSPR of AuNRs in our hybrid nanoparticles. This is further confirmed by the statistics obtained from analyzing a large number of similar isolated spots. Due to the variations of AuNR dimensions within the ensemble, different LSPR peak positions were obtained for different spots, which could be then correlated with the positions of the corresponding PL peaks. The result is shown in Fig. 3a and the obtained correlation in the broad spectral range (690–770 nm) clearly proves that the PL emission of AuNCs attached to AuNRs is controlled by the longitudinal LSPR of the AuNRs.

Using the data from Fig. 3a a histogram of PL peak positions can be created. Given the large extent of the underlying statistical sample (>450 points), such a histogram should reproduce the shape of the PL spectrum measured for an ensemble of AuNRs@AuNCs. The comparison is shown in Fig. 3b, where the PL spectrum of pure AuNCs is also shown. Looking first at the ensemble spectra (orange and blue lines), a redshift by ≈30 nm is observed for AuNRs@AuNCs compared with pure AuNCs. As already explained, this is caused by coupling of the PL to the LSPR of AuNRs 2, whose plasmonic band is shifted with respect to the emission band of AuNCs. Now, although the position of the main emission peak of AuNRs@AuNCs agrees very well with the constructed histogram, a non-negligible intensity appears also in the high energy tail of the PL spectrum (580–680 nm) where, however, no PL peaks were found during the analysis of isolated spots. Such a finding led us to a hypothesis that in addition to the emission from AuNCs coupled to AuNRs, the observed PL spectrum of AuNRs@AuNCs has another contribution from AuNCs which are not affected by AuNRs (denoted as non-coupled). Here we remind the thorough characterization of AuNRs@AuNCs in our previous report,[45] which showed that the purification of samples by centrifugation leaves a negligible amount of free (nonattached) AuNCs in the solution. Consequently, the non-coupled, high-energy contribution in the ensemble PL spectrum must also originate from the AuNCs attached to Au@SiO_2 NRs. The suggested picture of the two contributions is shown in Fig. 3c. We assume that the non-coupled AuNCs have the same PL spectrum as free AuNCs. The high energy shoulder of the AuNRs@AuNC spectrum (blue line) can thus be reproduced by a suitable normalization of the spectrum of pure AuNCs (orange line). The con-

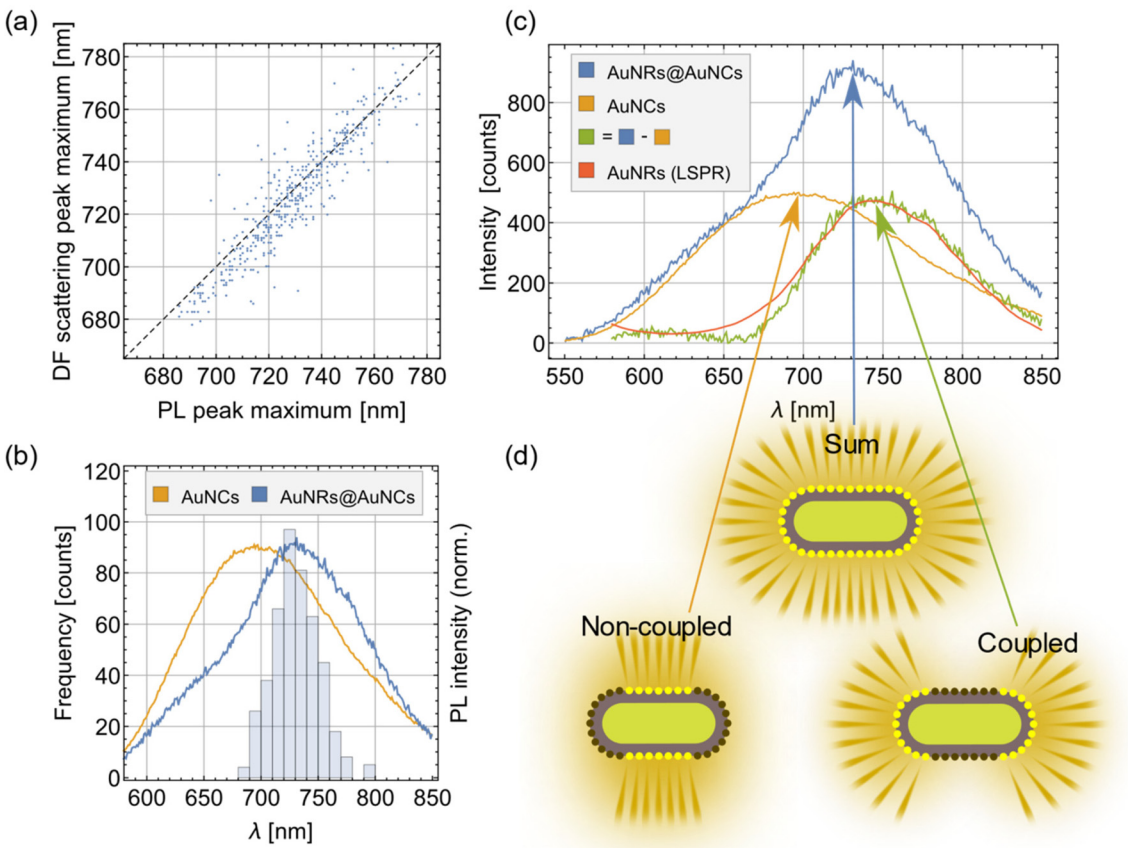

Fig. 3 (a) Correlation of PL and DF scattering peak positions obtained from single particle measurements of AuNRs@AuNCs prepared from AuNRs 2 with a 11 nm shell. (b) Comparison of the ensemble spectra of the same sample of AuNRs@AuNCs with a histogram of PL peak positions constructed from the data in (a). Ensemble PL spectrum of pure AuNCs is shown as a reference. (c) Suggested decomposition of the ensemble spectrum of AuNRs@AuNCs into "coupled" and "non-coupled" contributions. (d) Different positions of AuNCs attached to Au@SiO_2 NRs as an origin of the "coupled" and "non-coupled" contributions.

 This journal is © The Royal Society of Chemistry 2023

Open Access Article. Published on 09 January 2023. Downloaded on 5/9/2026 9:48:21 AM.
This article is licensed under a Creative Commons Attribution-NonCommercial 3.0 Unported Licence.

tribution of the coupled AuNCs can be then obtained by subtracting the non-coupled part from the original spectrum of AuNRs@AuNCs. The spectrum of the coupled AuNCs thus obtained (green line) can be directly compared with the longitudinal LSPR peak of AuNRs 2 (red line). The excellent overlap shown in Fig. 3c agrees well with our previous observations for isolated particles (Fig. 2 and S4†) and therefore serves as the first indication of the correctness of our hypothesis.

As already argued, both the coupled and non-coupled contributions to the overall spectrum of AuNRs@AuNCs must originate from AuNCs that are attached to Au@SiO_2 NRs. We suggest that the difference between the two groups of AuNCs is due to their different position on the surface of Au@SiO_2 NRs. Considering the inhomogeneous spatial profile of the Purcell factor around the AuNRs shown in Fig. 1b, a higher chance of coupling is expected for AuNCs located closer to the AuNR tips. Therefore, in Fig. 3d we suggest that the coupled and non-coupled contributions are from AuNCs resting at the tips and on the sides of Au@SiO_2 NRs, respectively. In the following we shall support this hypothesis with further evidence based on PL measurements.

Position-dependent plasmon-coupling of AuNCs on Au@SiO_2 NRs

First, we focus on the coupled contribution. Looking more closely on the map of the Purcell factor around the AuNR tip (Fig. 1b), we find that the area with high enhancement (coupling) potential has practically the same spherical symmetry as the tip of the AuNRs. Consequently, the relative number of AuNCs lying in the high Purcell factor region should decrease with the increasing distance of AuNCs from AuNRs – *i.e.*, with increasing SiO_2 shell thickness. The suggested difference between the thin and thick SiO_2 shells is shown in Fig. 4a and b, respectively.

The different ratios of the number of coupled and non-coupled AuNCs should be then also reflected in the PL spectra of the corresponding AuNRs@AuNCs. Starting from the model in Fig. 4a and b, let us first consider the ensemble PL spectra of AuNCs attached to AuNRs 2 with thin (5 nm) and thick (23.5 nm) SiO_2 shells – see Fig. 4c. Clearly, the shapes of the overall spectra of AuNRs@AuNCs (blue lines) are different for the two samples. Using the same disentanglement as in Fig. 3c, this can be explained by the different relative contributions of the coupled (red) and non-coupled (green) parts. As expected, the ratio between the coupled and non-coupled peaks is higher in the sample with a 5 nm shell compared to a 23.5 nm shell, indicating that more AuNCs were affected by the plasmonic resonance when attached closer to the AuNRs. As shown in Fig. 4d, this trend was further confirmed by measuring the PL spectra for samples within the whole range of SiO_2 shell thicknesses between 5 and 23.5 nm. Note that the spectra in Fig. 4d were normalized to the same intensity at 630 nm, which is where the influence of LSPR from AuNRs is the least (see the extinction spectrum of AuNRs 2 in Fig. S1†).

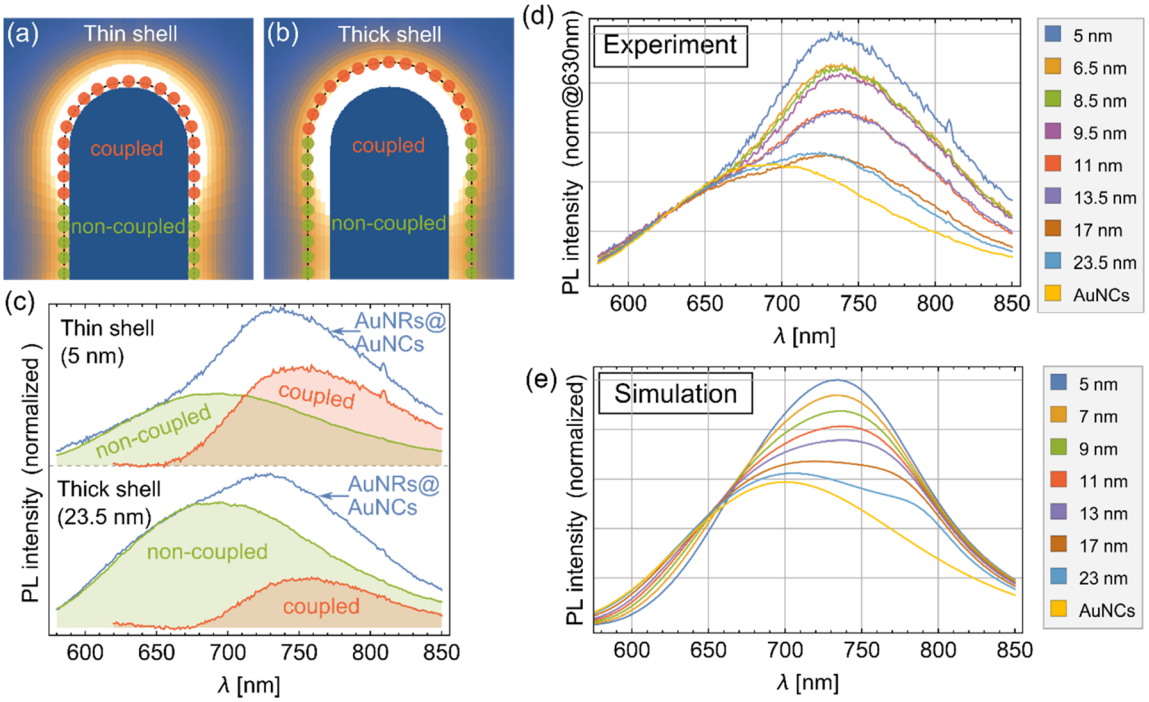

Fig. 4 Finding the position of coupled AuNCs. Schematic illustration of the relative number of coupled and non-coupled AuNCs attached to AuNRs with (a) a thin SiO_2 shell and (b) a thick SiO_2 shell. (c) Comparison of the PL spectral shapes of AuNRs@AuNCs prepared from AuNRs with a thin/thick SiO_2 shell explained as different contributions from the coupled and non-coupled AuNCs. (d) Comparison of the PL spectral shapes of AuNRs@AuNCs in the full range of SiO_2 shell thicknesses from 5 to 23.5 nm as measured in the experiment. (e) Comparison of the PL spectral shapes of AuNRs@AuNCs in the full range of SiO_2 shell thicknesses from 5 to 23.5 nm as calculated by BEM simulation.

Open Access Article. Published on 09 January 2023. Downloaded on 5/9/2026 9:48:21 AM.
This article is licensed under a Creative Commons Attribution-NonCommercial 3.0 Unported Licence.

Such normalization directly illustrates the increasing contribution from the coupled AuNCs in relationship with the fixed contribution from the non-coupled AuNCs with decreasing SiO_2 shell thickness. Moreover, due to the different spectral positions of the coupled and non-coupled peaks, their varying contribution causes varying spectral positions of the overall spectrum of AuNRs@AuNCs. As a result, the thinner the SiO_2 shell, the more redshifted is the spectrum of AuNRs@AuNCs. Such observation was finally also confirmed by calculating the PL spectra of AuNRs@AuNCs with comparable SiO_2 shell thicknesses using BEM simulations (see the ESI† for details of BEM simulations). The calculated spectra presented in Fig. 4e show the same trend as the experimental result in Fig. 4d, which confirms the coherence of our theory.

We now focus more on the non-coupled part of the spectra and prove that this contribution is from AuNCs placed on the sides of Au@SiO_2 NRs. To do so, we designed an experiment with two excitation wavelengths as shown in Fig. 5. In addition to an excitation at 405 nm, which was used in all the experiments presented so far, an excitation at 510 nm was used, which matches the transversal LSPR peak of AuNRs – see Fig. 5a. It is well known that the excitation light scattered by the LSPR is concentrated in the close vicinity of the plasmonic particles, which enables a stronger excitation of nearby fluorophores. In fact, this is the principle of plasmonic excitation enhancement discussed in our previous report.[45] For the transversal LSPR of AuNRs the region of the high excitation intensity is at the sides of the AuNRs – see the maps of calculated field enhancement around the AuNRs for excitation at 405 and 510 nm in Fig. 5b and c. As a result, measuring the PL spectra from the same sample of AuNRs@AuNCs using either of the excitation should make it possible to distinguish the contribution from AuNCs at the sides of Au@SiO_2 NRs. The result of PL measurements is shown in Fig. 5d, where the spectra collected at 405 nm (blue) and 510 nm (orange) excitation are directly compared for three samples of AuNRs@AuNCs and a reference sample of pure AuNCs. Note that while the shape of the PL spectrum of pure AuNCs remains practically identical regardless of the excitation, for AuNRs@AuNCs switching the excitation from 405 nm to 510 nm causes a blueshift of the spectra. Keeping in mind the results presented in Fig. 4, this blueshift can be explained as an increased contribution from the non-coupled fraction of AuNCs. To support this claim, we plotted a peak decomposition (analogous to the one in Fig. 4c) where the increased non-coupled PL emission under 510 nm excitation is directly shown – see Fig. S5 in the ESI.† In other

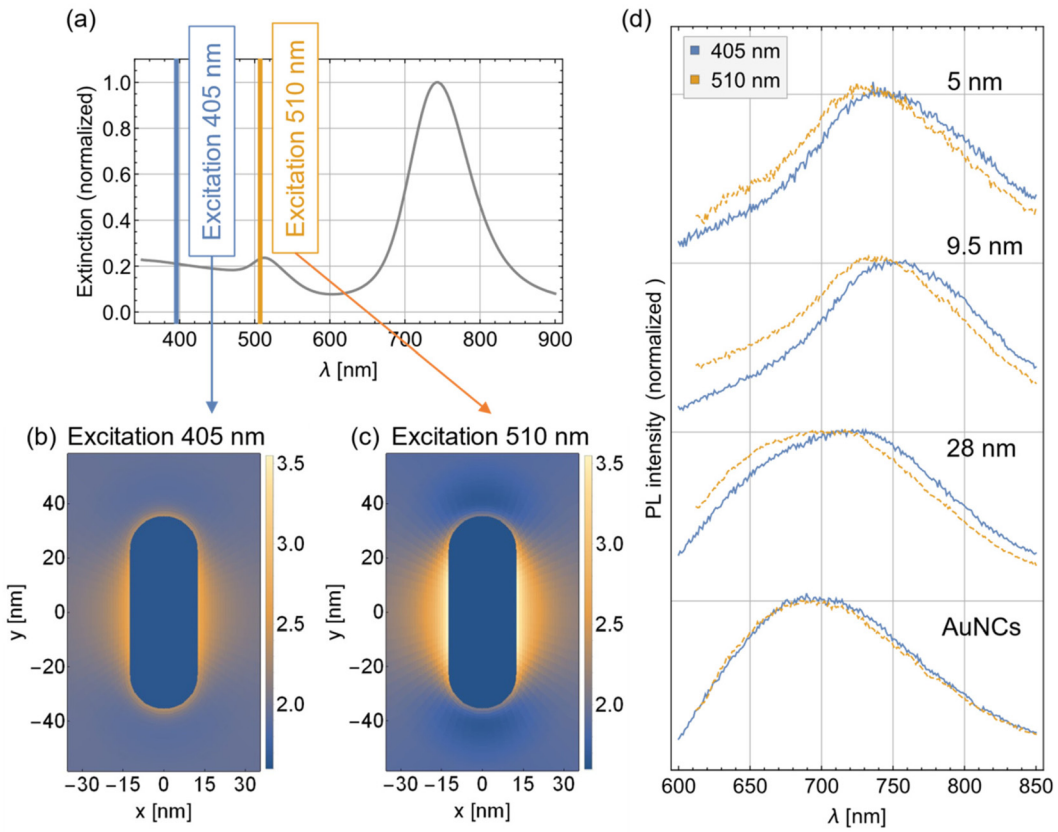

Fig. 5 Finding the position of non-coupled AuNCs. (a) In addition to an excitation at 405 nm, an excitation at 510 nm was used in the experiment which matches the transversal LSPR peak of AuNRs. (b) BEM simulation of electric field enhancement around the AuNRs at 405 nm excitation. (c) BEM simulation of electric field enhancement around the AuNRs at 510 nm excitation. (d) Comparison of the PL spectra of AuNRs@AuNCs under 405 nm (blue) and 510 nm (orange) excitation at different SiO_2 shell thicknesses (5, 9.5, and 28 nm). A reference sample of pure AuNCs is also shown.

This journal is © The Royal Society of Chemistry 2023

Open Access Article. Published on 09 January 2023. Downloaded on 5/9/2026 9:48:21 AM.
This article is licensed under a Creative Commons Attribution-NonCommercial 3.0 Unported Licence.

words, favoring the excitation of AuNCs at the sides of Au@SiO_2 NRs led to an increased intensity of the non-coupled part of the PL spectrum. We can therefore conclude that the non-coupled contribution must originate from the AuNCs placed at the sides of Au@SiO_2 NRs.

Assessment of the PL enhancement factor from PL spectra

The presented discrimination between the coupled and non-coupled AuNCs has an important consequence for their PL emission enhancement, as apparently only a certain fraction of the attached AuNCs can be influenced by AuNRs. Therefore, the specific position of AuNCs on Au@SiO_2 NRs represents another parameter to be considered in the PL enhancement studies. However, the experimental reality makes it almost impossible to measure the signal from the two contributions separately and the ensemble studies will always only provide averaged information. Yet, this problem can be circumvented by using the disentanglement introduced in Fig. 3c. Here, separation of the coupled and non-coupled parts of the overall PL spectrum enables calculating the photon count from the two groups of AuNCs. By estimating the number of AuNCs in either of the groups, the number of photons emitted by a single coupled *vs.* single non-coupled AuNC can be compared. Assuming that the non-coupled AuNCs are not affected by AuNRs at all, such a comparison directly yields the PL enhancement factor.

Following this idea, we performed the separation of the coupled and non-coupled contributions for all spectra shown in Fig. 4d and calculated the enhancement factors. The results presented in Fig. 6a show a monotonous tendency with the highest enhancement of ≈2.1× obtained for the 5 nm SiO_2 shell and decreasing down to ≈0.2× for the 23.5 nm shell. These data therefore suggest that the enhancement is only achieved for thin (<10 nm) shells and turns into quenching for thicker shells. Note that this calculation would not be possible if it was not for the offset between the LSPR of AuNRs 2 and the PL of AuNCs. As shown in Fig. S6 (in the ESI†), attaching AuNCs to the better matching AuNRs 1 yields the PL spectra of AuNRs@AuNCs that are very similar to the original spectrum of pure AuNCs, which makes the separation of the coupled and non-coupled contributions impossible.

However, keeping in mind the assumptions made on the way, the result presented in Fig. 6a should be taken with caution. First, the assumption that the non-coupled AuNCs are

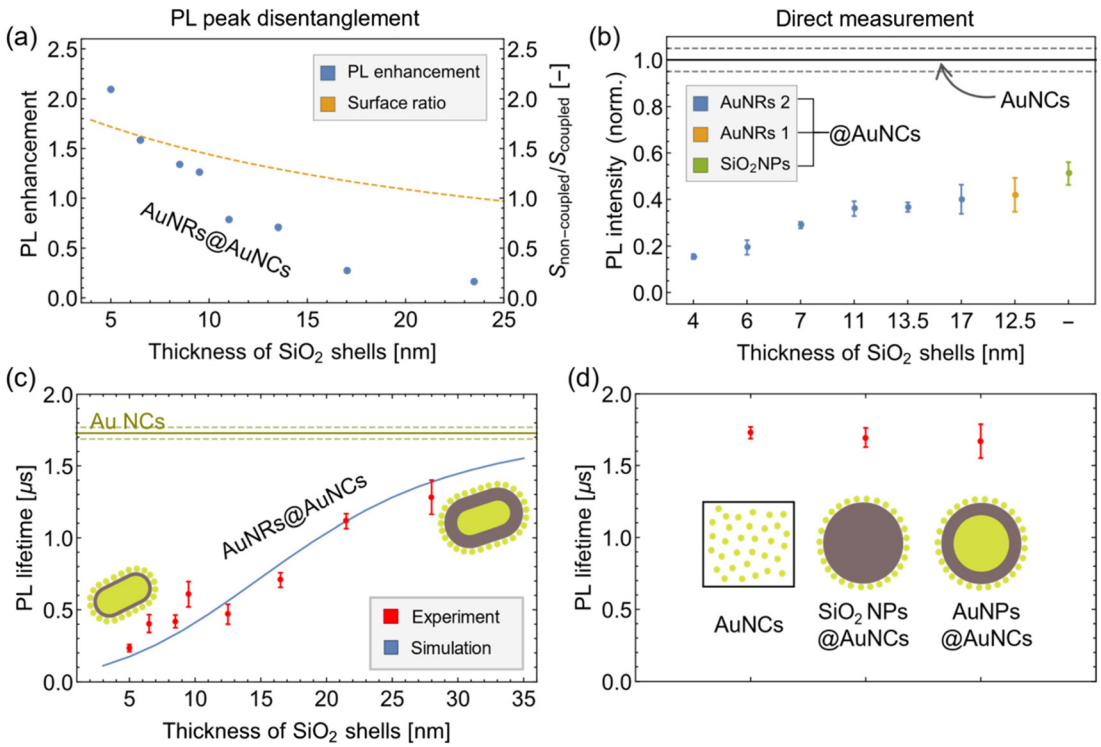

Fig. 6 Calculation of PL enhancement by two different methods. (a) Results obtained from the PL peak disentanglement into coupled and non-coupled parts show decreasing enhancement for increasing SiO_2 shell thickness. The model used for predicting the number of non-coupled and coupled AuNCs (orange line) shows a similar shell thickness dependence. (b) Normalized PL intensity obtained directly by measuring the signal from the calibrated samples of AuNRs@AuNCs. In addition to the samples based on AuNRs 2, a sample based on AuNRs 1 and on pure SiO_2 NPs was also studied (orange and green points, respectively). The horizontal gray lines represent a reference value of 1.00 ± 0.05 for the PL intensity of pure AuNCs. A reversed shell thickness dependence is observed compared to (a). Although different sets of Au@SiO_2 NR samples were used in (a) and (b), the range of shell thicknesses is comparable in both cases. (c) Dependence of the PL lifetime of AuNRs@AuNCs on SiO_2 shell thickness. The experimental data agree with the tendency predicted by BEM simulations. The horizontal yellow lines represent a reference value of 1.73 ± 0.04 μs for the PL lifetime of pure AuNCs. (d) PL lifetimes of the reference samples.

Open Access Article. Published on 09 January 2023. Downloaded on 5/9/2026 9:48:21 AM.
This article is licensed under a Creative Commons Attribution-NonCommercial 3.0 Unported Licence.

completely unaffected may not be true. Therefore, strictly speaking such a calculated enhancement only provides information about how many times the PL from the coupled AuNCs is stronger than the PL from the non-coupled AuNCs. More notably, the whole calculation is strongly dependent on the chosen model for the number of coupled and non-coupled AuNCs. In Fig. 6a a simple model was used, which assumes that the borderline between the two groups is always fixed in the transition plane where the body of AuNRs turns into its tip – see the details of the model in Fig. S7 (in the ESI†). With the homogeneous distribution of AuNCs on the surface of Au@SiO_2 NRs (confirmed by TEM imaging), the ratio between the number of non-coupled and coupled AuNCs can be calculated as the ratio between the areas of the corresponding parts of SiO_2 shells. In the proposed model, however, this ratio changes rapidly with the shell thickness because the tip area of Au@SiO_2 NR increases much faster than the area of its sides – see the dependence of the ratio on shell thickness in Fig. 6a. Apparently, the calculated enhancement follows a similar dependence on the shell thickness as the predicted number ratio between the non-coupled and coupled AuNCs. Given the uncertainty in the selection of the model, this represents a significant drawback of such enhancement calculations.

Therefore, we designed an alternative experiment where the PL enhancement was measured directly. For this, a set of calibrated samples was prepared, where the number of AuNCs was accurately determined using neutron activation radiolabeling as reported previously.[45] Besides the samples based on AuNRs 2 (SiO_2 shells ranging from 4 to 17 nm), a calibrated sample based on AuNRs 1 with a 12.5 nm SiO_2 shell was also prepared to include a case with optimal LSPR–PL overlap. Apart from pure AuNCs, spherical SiO_2 nanoparticles attached with AuNCs (SiO_2NPs@AuNCs) were also prepared as a reference so that the effect of fixing AuNCs on the SiO_2 surface could be assessed. Thanks to the calibration, the measured PL spectra could be related to the total number of AuNCs, which then enabled a direct comparison of the PL intensity per AuNC between the samples. The result is shown in Fig. 6b, where the PL intensity of the reference sample of pure AuNCs, was normalized to 1. In contrast to our expectations, a reduced PL intensity was observed for all the samples of AuNRs@AuNCs compared to pure AuNCs, indicating that instead of enhancement, PL quenching was induced by AuNRs. The shell thickness dependency is again monotonous with the strongest quenching found for the sample with the thinnest (4 nm) SiO_2 shell (≈0.15×) and the weakest quenching (≈0.40×) found for the sample with a 17 nm shell. A slightly weaker quenching (≈0.42×) was then obtained for the sample prepared from AuNRs 1 with a 12.5 nm SiO_2 shell. Such observation suggests that the information extracted from this experiment is still not complete, because if the PL was merely quenched then using AuNRs with better LSPR–PL overlap should cause stronger quenching than AuNRs with an LSPR offset from AuNC emission. Moreover, a significantly reduced PL intensity (≈0.49×) was obtained even for the reference sample of SiO_2NPs@AuNCs, implying that most of the quenching might be actually due to the SiO_2 surface.

To gain more insight into how the AuNRs and SiO_2 surface affect the emission of AuNCs, we measured the PL lifetimes of the prepared samples. First, the SiO_2 shell thickness dependency was studied for AuNRs@AuNCs based on AuNRs 2. According to the definition of PL lifetime, both the Purcell enhancement and non-radiative quenching should lead to a reduction of the lifetime. The stronger the particular effect the stronger the impact on the lifetime is expected. This was confirmed by our measurement, and the results are shown in Fig. 6c. The decrease of the lifetime from the original value of ≈1.73 μs for pure AuNCs is relatively monotonous and goes from ≈1.28 μs for AuNRs@AuNCs with a 28 nm shell down to ≈0.23 μs for AuNRs@AuNCs with a 5 nm shell. This dataset also serves as a good opportunity to verify the accuracy of our BEM simulations. The calculated PL lifetime is shown in Fig. 6c as a blue line and shows a good agreement with the experimental data.

Fig. 6d shows the measured PL lifetimes for three reference samples – pure AuNCs, SiO_2NPs@AuNCs, and AuNCs attached to spherical Au nanoparticles (AuNPs@AuNCs) – which were compared to see the effect of the SiO_2 surface and the effect of gold nanoparticles whose LSPR (at 510 nm) is far from the emission of AuNCs. The observation of a nearly identical PL lifetime in all three cases means that neither silica nor gold by themselves cause an increase of the radiative or nonradiative rate in AuNCs. In the case of AuNPs@AuNCs this confirms that a sufficient overlap of LSPR and PL is required to affect the emission.

In the case of SiO_2NPs@AuNCs, important deduction can be obtained by combing data from Fig. 6b and d. While the PL intensity is reduced to half, the PL lifetime is not changed compared to the initial solution of AuNCs. The decrease in the PL intensity of SiO_2NPs@AuNCs can then be explained by an increased number of AuNCs switched into a non-luminescent ("dark") state upon their attachment to the SiO_2 surface. Such quenching can be due to charge carriers localized on the SiO_2 surface close to AuNCs.[60] Alternatively, the PL of AuNCs can be switched off by forming aggregates during attachment to SiO_2.[61] Yet, from the theoretical point of view the effect of the SiO_2 shell can be separated from the effect of LSPR and the achievable PL enhancement/quenching can be studied independently. Still, there is one more variable left that has not been accounted for in the experiment presented in Fig. 6b, which is the reabsorption of the emitted PL photons by other AuNRs in the bulk solution.

Real enhancement factor from AuNC-concentration dependent PL spectra

Another approach to PL enhancement measurement was therefore used in the last experiment. In this method, which we first introduced in our previous report,[45] three solutions are always studied at the same time – pure AuNCs, AuNRs@AuNCs, and AuNCs mixed with AuNRs but not attached to them (denoted as AuNRs + AuNCs). The measure-

 This journal is © The Royal Society of Chemistry 2023

Open Access Article. Published on 09 January 2023. Downloaded on 5/9/2026 9:48:21 AM.
This article is licensed under a Creative Commons Attribution-NonCommercial 3.0 Unported Licence.

ment then proceeds in many steps, where the number of AuNCs added to each sample is gradually increased. Thanks to the thorough characterization of AuNRs@AuNCs summarized at the beginning of this section, these steps can be designed in such a way that the number of AuNCs used ranges from far below to far above the attachment saturation (*i.e.*, the maximum achievable surface coverage of Au@SiO_2NRs by AuNCs). The dataset thus created yields a dependency of the PL intensity on the number (concentration) of AuNCs, whose slope has the meaning of PL intensity per AuNC (at given AuNC loading).

The results of four such measurements are shown in Fig. 7. The same samples of Au@SiO_2NRs (and SiO_2NPs) were used here as in the experiment presented in Fig. 6. The most important features of the obtained data can be described in the example of AuNRs@AuNCs based on AuNRs 2 with a 6 nm shell (Fig. 7a). The situation for pure AuNCs and AuNRs + AuNCs is quite simple as the PL intensity increases linearly with the concentration of AuNCs. However, the slope of this increase is smaller for AuNRs + AuNCs, proving that the reabsorption of the PL photons takes place in the bulk solution containing AuNRs. Now, for AuNRs@AuNCs two regions must be distinguished. First, at small AuNC concentrations all AuNCs introduced in the solution are attached to Au@SiO_2NRs. Then attachment saturation is reached (the region of expected saturation lies between the two vertical dashed lines in Fig. 7a) upon which no more additional AuNCs can be attached and remain free in the solution. Consequently, the slope of increase of the PL intensity changes, from which the effect of AuNC attachment to Au@SiO_2NRs can be deduced. In Fig. 7a the slope for AuNRs@AuNCs is higher in the saturated region than in the non-saturated region, indicating that the PL of AuNCs was quenched by AuNRs in this sample (≈0.6× enhancement factor can be calculated).

The situation is different for a sample of AuNRs@AuNCs based on AuNRs 2 with a 13.5 nm shell as shown in Fig. 7b. This time the slope of the dependence (*i.e.*, the PL intensity per AuNC) slightly decreases after reaching the saturation point, showing that in this case attaching AuNCs to Au@SiO_2NRs resulted in PL enhancement. Still, this enhancement (≈1.2×) is too small to fully compensate for the reabsorption in the bulk solution (note that the PL intensity remains lower for AuNRs@AuNCs compared to pure AuNCs even at the saturation limit in Fig. 7b). It is also noted that the increase of PL intensity in the non-saturated region is not linear but rather accelerates with increasing concentration of AuNCs. The source of this nonlinearity is not clear, but arguably it is

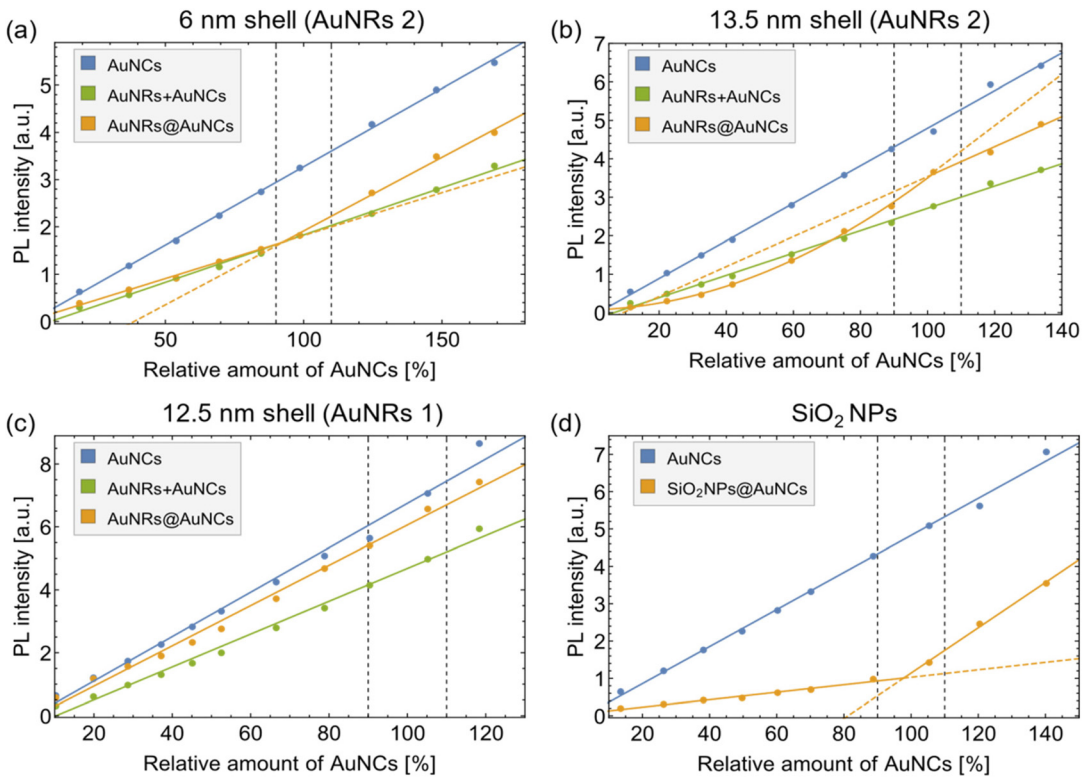

Fig. 7 Results of PL intensity enhancement in AuNCs attached to Au@SiO_2 NRs (AuNRs@AuNCs; orange) compared to free AuNCs (blue) and AuNCs mixed with but not attached to AuNRs (AuNRs + AuNCs; green) for the samples prepared from (a) AuNRs 2 with a 6 nm shell, (b) AuNRs 2 with a 13.5 nm shell, and (c) AuNRs 1 with a 12.5 nm shell. (d) An analogous measurement for a reference sample of pure SiO_2 NPs. In all graphs, the horizontal axes were normalized to the maximum loading capacity of the used Au@SiO_2 NRs. The dashed vertical lines indicate the range where attachment saturation is expected (100% ± standard deviation). The two dashed orange lines represent the tangents of the fits of data in the saturated and non-saturated regions of AuNRs@AuNCs (SiO_2NPs@AuNCs), respectively.

Open Access Article. Published on 09 January 2023. Downloaded on 5/9/2026 9:48:21 AM.
This article is licensed under a Creative Commons Attribution-NonCommercial 3.0 Unported Licence.

somehow related to a mild aggregation of AuNRs@AuNCs caused by surface charge neutralization as discussed in our previous report.[45] Nevertheless, strictly speaking, the only important region of the measured data is close to the saturation point. Assuming that the colloidal state of the particles does not change rapidly here, all we need is to compare the tangent of the non-saturated dependence and the saturated dependence, both evaluated at the saturation point (tangents indicated as dashed lines in all graphs in Fig. 7). The enhancement is then calculated simply as a ratio of the non-saturated to the saturated tangent.

This principle only failed for AuNRs@AuNCs based on AuNRs 1 with a 12.5 nm shell. As shown in Fig. 7c, there is no apparent change of the slope in the saturation region here. Still, note that the PL intensity is considerably higher than for AuNRs + AuNCs at all AuNC concentrations. Therefore, rather than to the absence of enhancement this might be attributed to the small amount of datapoints in the saturated region. Comparing the slopes for AuNRs@AuNCs and AuNRs + AuNCs we can obtain an alternative enhancement factor of ≈1.3×. Finally, the reference sample of SiO_2NPs@AuNCs was also studied in this experiment. The result presented in Fig. 7d confirms the finding from Fig. 6 that the significantly decreased PL intensity of AuNCs is caused solely by their attachment to the silica surface. The ratio of tangents calculated from the data in Fig. 7d yields a factor of ≈0.2×, which is even less than what was found in Fig. 6.

As for the PL enhancement, the combined information obtained from all the presented experiments can be viewed in two ways – what can be achieved within the combination of AuNRs and AuNCs theoretically and what is achieved in reality. The reality evidenced by the data in Fig. 7 clearly shows that even in the cases where PL enhancement was stated, the obtained PL intensity does not exceed the level for pure AuNCs. Therefore, attaching AuNCs to AuNRs *via* a SiO_2 spacer for emission enhancement does not seem to be beneficial for practical purposes. Yet, as shown throughout this section, the main drawbacks of our experimental setting result from the PL loss upon attachment of AuNCs on the SiO_2 spacer and from the reabsorption of PL photons in bulk solutions containing AuNRs. These limitations could be in principle circumvented if a different spacer was used, and if the particles were arranged in a thin layer where the reabsorption should be negligible. Therefore, it still makes sense to look at the theoretical capabilities of AuNRs@AuNCs.

Theoretical enhancement capability of optimized AuNRs@AuNCs

We have performed a set of BEM simulations for AuNRs@AuNCs with different parameters (see the ESI† for the full description of the model used). Apart from the spacer thickness, the AuNR volume (V) and aspect ratio (AR) were also varied. As discussed above, varying the AR causes a shift of the longitudinal LSPR band of AuNRs. Calculating the PL enhancement (ξ) as a function of the AR therefore enables the evaluation of the effect of LSPR–PL band overlap/mismatch created for AuNRs 1 and AuNRs 2, respectively. Fig. 8a shows the result calculated for a range of AuNRs with a fixed particle volume (16 304 nm^3; corresponds to AuNRs 2) and SiO_2 shell thickness (5 nm), and the AR varying from 2.5 to 3.5. In this calculation the AuNC QY was set as η_0 = 7.8%, which is a value that we measured directly for a sample of pure AuNCs. As expected, the highest PL enhancement (≈2.3×) is predicted for AuNRs with AR = 2.8, whose LSPR matches the PL band of

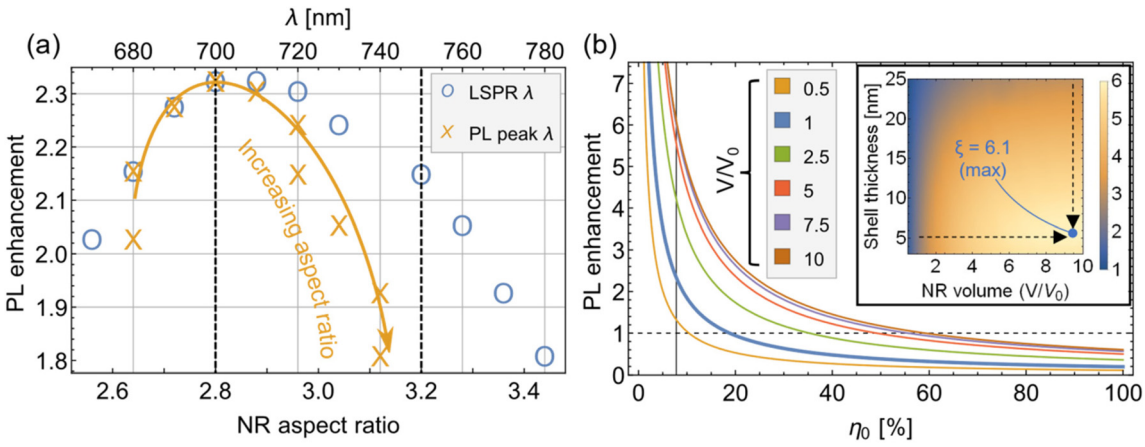

Fig. 8 Calculated theoretical PL enhancement in AuNRs@AuNCs as a function of (a) AuNR aspect ratio (at a fixed AuNR volume V_0 = 16 304 nm^3, an AuNC QY η_0 = 7.8%, and 5 nm SiO_2 shell thickness) and (b) AuNC QY η_0 (for a set of different AuNR volumes, at optimal AuNR aspect ratio ensuring perfect PL–LSPR match, and 5 nm SiO_2 shell thickness). In (a) the upper horizontal axis shows the peak longitudinal LSPR wavelength of AuNRs with the aspect ratio given by the lower horizontal axis. By looking at the upper horizontal axis, the orange crosses in (a) show the peak PL wavelength of AuNCs attached to AuNRs with varying aspect ratios (each orange cross corresponds to the blue circle at the same PL enhancement level). The two dashed vertical lines indicate the incidence of theoretical results for AuNRs 1 and AuNRs 2, respectively. The vertical line in (b) indicates the measured QY of AuNCs 7.8%, and the dashed horizontal line indicates the limit of positive PL enhancement (>1). The inset in (b) extends the data from the main plot by the dependence on the SiO_2 shell thickness (calculated for the measured AuNC QY η_0 = 7.8%).

This journal is © The Royal Society of Chemistry 2023

Open Access Article. Published on 09 January 2023. Downloaded on 5/9/2026 9:48:21 AM.
This article is licensed under a Creative Commons Attribution-NonCommercial 3.0 Unported Licence.

AuNCs at 700 nm (see the LSPR wavelength corresponding to a particular AR on the upper horizontal axis of Fig. 8a). This represents the optimal case of using AuNRs 1. However, increasing the AR to 3.2, which represents the case of using AuNRs 2 with LSPR at 750 nm, only decreases the predicted enhancement to ≈2.15×. Apart from the PL enhancement (blue circles), Fig. 8a also shows the calculated PL peak positions for the same set of AuNRs@AuNCs (orange crosses – the PL peak wavelength was found on the upper horizontal axis). Comparison of the two results shows that the ensemble PL band of AuNRs@AuNCs cannot follow the LSPR band of AuNRs indefinitely and the larger the offset the smaller the enhancement.

Two important conclusions can be made based on the data presented in Fig. 8a. First, even a quite large LSPR–PL offset does not reduce the PL enhancement too far below the maximum value. Second, even the maximum theoretical PL enhancement is relatively small for the given combination of AuNRs, AuNCs and the SiO_2 spacer. Therefore, the AuNR volume was considered as an additional parameter in the calculations to extend the options for achieving a higher enhancement factor. It is well known from the basic principles of plasmonics that with an increasing particle volume the ratio between light scattering and absorption at the resonant wavelength also increases.[62] We expected that as a result the ratio between the external and total Purcell factors would increase and the achievable enhancement would be higher. This was confirmed by the simulations as shown in Fig. 8b. Here the calculated PL enhancement is plotted as a function of the QY of AuNCs (η_0) for a set of different AuNR volumes. A fixed shell thickness of 5 nm was used in all the cases and the optimal AuNR aspect ratio of 2.8 was individually adjusted to compensate the small LSPR shift caused by the varying AuNR size (thus creating a perfect PL–LSPR match for all AuNR volumes). We found that PL enhancement increases with the AuNR volume and this trend continues until an order of magnitude increase of the original volume ($V/V_0 \sim 10$) is reached, after which increasing the AuNR size no longer seems to be beneficial. Naturally, the smaller the input QY of pure AuNCs, the larger enhancement factors can be achieved. For our sample of AuNCs with the QY measured as η_0 = 7.8%, the calculations predict an increase of ξ from 2.3× (at the original AuNR volume) to 6.1× (at the 10 times increased AuNR volume). Fixing the AuNC QY at 7.8%, the calculations further predict that the optimal SiO_2 shell thickness is 5 nm (see the inset of Fig. 8b), which justifies the use of this spacer in all the previous calculations shown in Fig. 8. Thus, increasing the AuNR volume seems to be a possible way of achieving a PL emission enhancement whose magnitude is comparable to the excitation enhancement reported previously.[45] Importantly, note that even the largest AuNRs considered (V/V_0 = 10) can still be prepared by the conventional seeded growth method, as their dimensions would be ≈120 × 45 nm. Nevertheless, such an experimental demonstration exceeds the scope of this study and we will focus on this problem in our following work.

Conclusion

This study provides a comprehensive description and spectroscopic study of a single-element system based on plasmonic gold nanorods bearing ultra-small fluorescent gold nanoclusters. The geometrical and optical tunability of the system enabled us to identify leading principles determining the advantages and limits of plasmonic emission enhancement in similar systems. We benefit from the extraordinary degree of structural control in our hybrid nanoparticles and characterize the subtle balance between emission enhancement and quenching. We show, for example, that not just the separation distance but also the specific position of AuNCs on the surface of AuNRs play an important role in PL–LSPR coupling. By careful evaluation of the PL spectra of AuNRs@AuNCs, we managed to separate the coupled and non-coupled parts and assigned it to AuNCs attached to the tips and sides of AuNRs, respectively. We further developed a general way of measuring the PL enhancement, which accounts even for the reabsorption of the emitted PL photons by AuNRs in the bulk solution and thus enables the assessment of the PL enhancement effect itself.

In addition to the spectroscopic characterization, we performed BEM calculations which showed an excellent match with the experimental results. Among other results, BEM calculations helped us to identify a potential improvement of the emission enhancement by increasing the AuNR volume. We emphasize that the good match between our experimental data and simulations suggests the reliability of the predicted results even for samples that were not examined in our experiments.

We critically compared the possibilities of emission enhancement determined in this work and excitation enhancement which we observed experimentally for the same combination of AuNRs and AuNCs in our previous study.[45] We found that even the maximum emission enhancement that can be achieved theoretically is lower than the excitation enhancement and does not improve the applicability of the AuNCs as luminescent particles.

One possible way to increase the enhancement factor is to avoid the non-coupled particles on the side of AuNRs by growing a silica shell on the tips of NRs only. Such a dumbbell-shaped composite was recently prepared to demonstrate the increased efficiency of the SERS effect by Meyer and Murphy.[63] Other approaches can be used as well, for example, tip-selective modification by fluorescent molecules.[64] Eventual demonstration of the fluorescence enhancement improvement in the AuNRs@AuNC composite with the dumbbell coverage by silica would require another laborious investigation.

Finally, we believe that the methodological approach used in this study is relevant for a variety of analogous studies and can be applied to any plasmonic system based on gold nanorods optically tuned for the emission enhancement of a suitable fluorophore.

Open Access Article. Published on 09 January 2023. Downloaded on 5/9/2026 9:48:21 AM. This article is licensed under a Creative Commons Attribution-NonCommercial 3.0 Unported Licence.

Conflicts of interest

There are no conflicts to declare.

Acknowledgements

The authors are grateful to Dr Jiri Mizera (Nuclear Physics Institute of the CAS) for his help with neutron activation analysis. The authors acknowledge support from the Czech Science Foundation project no. 18-12533S. P. C. and K. K. acknowledge support from the European Regional Development Fund, OP RDE, Project: CARAT (no. CZ.02.1.01/0.0/0.0/16_026/0008382).

References

1 G. Pramanik, J. Humpolickova, J. Valenta, P. Kundu, S. Bals, P. Bour, M. Dracinsky and P. Cigler, *Nanoscale*, 2018, **10**, 3792–3798.
2 S. E. Crawford, C. M. Andolina, A. M. Smith, L. E. Marbella, K. A. Johnston, P. J. Straney, M. J. Hartmann and J. E. Millstone, *J. Am. Chem. Soc.*, 2015, **137**, 14423–14429.
3 J. Xie, Y. Zheng and J. Y. Ying, *J. Am. Chem. Soc.*, 2009, **131**, 888–889.
4 K. G. Stamplecoskie, Y.-S. Chen and P. V. Kamat, *J. Phys. Chem. C*, 2014, **118**, 1370–1376.
5 L. Shang, R. M. Dörlich, S. Brandholt, R. Schneider, V. Trouillet, M. Bruns, D. Gerthsen and G. Ulrich Nienhaus, *Nanoscale*, 2011, **3**, 2009–2014.
6 J. Zheng, C. Zhou, M. Yu and J. Liu, *Nanoscale*, 2012, **4**, 4073–4083.
7 J. Xu and L. Shang, *Chin. Chem. Lett.*, 2018, **29**, 1436–1444.
8 I. L. Garzón, J. A. Reyes-Nava, J. I. Rodríguez-Hernández, I. Sigal, M. R. Beltrán and K. Michaelian, *Phys. Rev. B: Condens. Matter Mater. Phys.*, 2002, **66**, 073403.
9 X.-K. Wan, S.-F. Yuan, Z.-W. Lin and Q.-M. Wang, *Angew. Chem.*, 2014, **126**, 2967–2970.
10 P. Crespo, R. Litrán, T. C. Rojas, M. Multigner, J. M. de la Fuente, J. C. Sánchez-López, M. A. García, A. Hernando, S. Penadés and A. Fernández, *Phys. Rev. Lett.*, 2004, **93**, 087204.
11 M. Agrachev, S. Antonello, T. Dainese, M. Ruzzi, A. Zoleo, E. Aprà, N. Govind, A. Fortunelli, L. Sementa and F. Maran, *ACS Omega*, 2017, **2**, 2607–2617.
12 J. Olesiak-Banska, M. Waszkielewicz, P. Obstarczyk and M. Samoc, *Chem. Soc. Rev.*, 2019, **48**, 4087–4117.
13 N. Schaeffer, B. Tan, C. Dickinson, M. J. Rosseinsky, A. Laromaine, D. W. McComb, M. M. Stevens, Y. Wang, L. Petit, C. Barentin, D. G. Spiller, A. I. Cooper and R. Lévy, *Chem. Commun.*, 2008, 3986–3988.
14 Z. Wu and R. Jin, *Nano Lett.*, 2010, **10**, 2568–2573.
15 L.-Y. Chen, C.-W. Wang, Z. Yuan and H.-T. Chang, *Anal. Chem.*, 2015, **87**, 216–229.
16 S. Palmal and N. R. Jana, *Wiley Interdiscip. Rev.: Nanomed. Nanobiotechnol.*, 2014, **6**, 102–110.
17 G. Pramanik, K. Kvakova, M. A. Thottappali, D. Rais, J. Pfleger, M. Greben, A. El-Zoka, S. Bals, M. Dracinsky, J. Valenta and P. Cigler, *Nanoscale*, 2021, **13**, 10462–10467.
18 G. Zuber, E. Weiss and M. Chiper, *Nanotechnology*, 2019, **30**, 352001.
19 A. Cantelli, G. Battistelli, G. Guidetti, J. Manzi, M. Di Giosia and M. Montalti, *Dyes Pigm.*, 2016, **135**, 64–79.
20 F. Wen, Y. Dong, L. Feng, S. Wang, S. Zhang and X. Zhang, *Anal. Chem.*, 2011, **83**, 1193–1196.
21 L. Shang, L. Yang, F. Stockmar, R. Popescu, V. Trouillet, M. Bruns, D. Gerthsen and G. Ulrich Nienhaus, *Nanoscale*, 2012, **4**, 4155–4160.
22 J. Valenta, M. Greben, G. Pramanik, K. Kvakova and P. Cigler, *Phys. Chem. Chem. Phys.*, 2021, **23**, 11954–11960.
23 C.-A. J. Lin, T.-Y. Yang, C.-H. Lee, S. H. Huang, R. A. Sperling, M. Zanella, J. K. Li, J.-L. Shen, H.-H. Wang, H.-I. Yeh, W. J. Parak and W. H. Chang, *ACS Nano*, 2009, **3**, 395–401.
24 J. Wang, G. Zhang, Q. Li, H. Jiang, C. Liu, C. Amatore and X. Wang, *Sci. Rep.*, 2013, **3**, 1157.
25 Y. Zheng, L. Lai, W. Liu, H. Jiang and X. Wang, *Adv. Colloid Interface Sci.*, 2017, **242**, 1–16.
26 A. S. K. Kumar and W.-L. Tseng, *Anal. Methods*, 2020, **12**, 1809–1826.
27 A. Cantelli, G. Guidetti, J. Manzi, V. Caponetti and M. Montalti, *Eur. J. Inorg. Chem.*, 2017, 5068–5084.
28 R. Xie and X. Peng, *Angew. Chem., Int. Ed.*, 2008, **47**, 7677–7680.
29 D. Gao, P. Zhang, Z. Sheng, D. Hu, P. Gong, C. Chen, Q. Wan, G. Gao and L. Cai, *Adv. Funct. Mater.*, 2014, **24**, 3897–3905.
30 B. L. Wehrenberg, C. Wang and P. Guyot-Sionnest, *J. Phys. Chem. B*, 2002, **106**, 10634–10640.
31 T. Torimoto, S. Ogawa, T. Adachi, T. Kameyama, K. Okazaki, T. Shibayama, A. Kudo and S. Kuwabata, *Chem. Commun.*, 2010, **46**, 2082–2084.
32 T. Ming, H. Chen, R. Jiang, Q. Li and J. Wang, *J. Phys. Chem. Lett.*, 2012, **3**, 191–202.
33 R. Jiang, B. Li, C. Fang and J. Wang, *Adv. Mater.*, 2014, **26**, 5274–5309.
34 Z. Yang, W. Ni, X. Kou, S. Zhang, Z. Sun, L.-D. Sun, J. Wang and C.-H. Yan, *J. Phys. Chem. C*, 2008, **112**, 18895–18903.
35 J. Ki Kim and D.-J. Jang, *J. Mater. Chem. C*, 2017, **5**, 6037–6046.
36 X. Yang, Y. Zhuo, S. Zhu, Y. Luo, Y. Feng and Y. Xu, *Biosens. Bioelectron.*, 2015, **64**, 345–351.
37 X. Feng, T. Han, Y. Xiong, S. Wang, T. Dai, J. Chen, X. Zhang and G. Wang, *ACS Sens.*, 2019, **4**, 1633–1640.
38 H. Qin, D. Ma and J. Du, *Spectrochim. Acta, Part A*, 2018, **189**, 161–166.
39 H. Kong, Y. Lu, H. Wang, F. Wen, S. Zhang and X. Zhang, *Anal. Chem.*, 2012, **84**, 4258–4261.
40 L. Qin, X. He, L. Chen and Y. Zhang, *ACS Appl. Mater. Interfaces*, 2015, **7**, 5965–5971.

 This journal is © The Royal Society of Chemistry 2023

Open Access Article. Published on 09 January 2023. Downloaded on 5/9/2026 9:48:21 AM.
This article is licensed under a Creative Commons Attribution-NonCommercial 3.0 Unported Licence.

41 X. Su, B. Fu and J. Yuan, *Mater. Lett.*, 2017, **188**, 111–114.
42 H. Zhang, P. Liu, H. Wang, X. Ji, M. Zhao and Z. Song, *Anal. Bioanal. Chem.*, 2021, **413**, 1541–1547.
43 J.-M. Liu, J.-T. Chen and X.-P. Yan, *Anal. Chem.*, 2013, **85**, 3238–3245.
44 C.-W. Chen, C.-H. Wang, C.-M. Wei, C.-Y. Hsieh, Y.-T. Chen, Y.-F. Chen, C.-W. Lai, C.-L. Liu, C.-C. Hsieh and P.-T. Chou, *J. Phys. Chem. C*, 2010, **114**, 799–802.
45 O. Pavelka, K. Kvakova, J. Vesely, J. Mizera, P. Cigler and J. Valenta, *Nanoscale*, 2022, **14**, 3166–3178.
46 K. Matsuzaki, H.-W. Liu, S. Götzinger and V. Sandoghdar, *ACS Photonics*, 2021, **8**, 1508–1521.
47 G. Pramanik, A. Keprova, J. Valenta, V. Bocan, K. Kvaková, L. Libusova and P. Cigler, *J. Visualized Exp.*, 2020, **157**, e60388.
48 B. Nikoobakht and M. A. El-Sayed, *Chem. Mater.*, 2003, **15**, 1957–1962.
49 O. Pavelka, S. Dyakov, J. Veselý, A. Fučíková, H. Sugimoto, M. Fujii and J. Valenta, *Nanoscale*, 2021, **13**, 5045–5057.
50 J. A. Edgar, A. M. McDonagh and M. B. Cortie, *ACS Nano*, 2012, **6**, 1116–1125.
51 I. Gorelikov and N. Matsuura, *Nano Lett.*, 2008, **8**, 369–373.
52 I. A. M. Ibrahim, A. A. F. Zikry and M. A. Sharaf, *J. Am. Sci.*, 2010, **6**, 985–989.
53 J. Turkevich, P. C. Stevenson and J. Hillier, *Discuss. Faraday Soc.*, 1951, **11**, 55–75.
54 J. Valenta and M. Greben, *AIP Adv.*, 2015, **5**, 047131.
55 W. Becker, *J. Microsc.*, 2012, **247**, 119–136.
56 F. J. García de Abajo and A. Howie, *Phys. Rev. B: Condens. Matter Mater. Phys.*, 2002, **65**, 115418.
57 U. Hohenester and A. Trügler, *Comput. Phys. Commun.*, 2012, **183**, 370–381.
58 J. Waxenegger, A. Trügler and U. Hohenester, *Comput. Phys. Commun.*, 2015, **193**, 138–150.
59 T. Ming, L. Zhao, Z. Yang, H. Chen, L. Sun, J. Wang and C. Yan, *Nano Lett.*, 2009, **9**, 3896–3903.
60 C. Galland, Y. Ghosh, A. Steinbrück, M. Sykora, J. A. Hollingsworth, V. I. Klimov and H. Htoon, *Nature*, 2011, **479**, 203–207.
61 C. Dai, C. Yang and X. Yan, *Nano Res.*, 2018, **11**, 2488–2497.
62 S. A. Maier, *Plasmonics: Fundamentals and Applications*, Springer, Berlin, 2007.
63 S. M. Meyer and C. J. Murphy, *Nanoscale*, 2022, **14**, 5214–5226.
64 D. Botequim, I. I. R. Silva, S. G. Serra, E. P. Melo, D. M. F. Prazeres, S. M. B. Costa and P. M. R. Paulo, *Nanoscale*, 2020, **12**, 6334–6345.